Published in final edited form as:
Surf Coat Technol. 2021 May 25; 414: . doi:10.1016/j.surfcoat.2021.127119.

Wettability and *in-vitro* study of titanium surface profiling prepared by electrolytic plasma processing

Wisanu Boonrawd[a], **Kamal R. Awad**[a,b], **Venu Varanasi**[a,b], **Efstathios I. Meletis**[a,*]

[a]Department of Materials Science and Engineering, The University of Texas at Arlington, Arlington, TX 76019, USA

[b]Bone Muscle Research Center, The University of Texas at Arlington, Arlington, TX 76019, USA

Abstract

Electrolytic plasma processing (EPP) was used to create hydrophilic surface profiles on titanium. The wettability, surface morphology characteristics and chemical composition of the treated samples were studied as a function of EPP processing parameters. The EPP profiled surfaces comprised of a characteristic “hills and valleys” morphology because of continuous surface melting and freezing cycles. A bimodal surface profile was produced with 2–3 μm height hills and valleys with nano-roughness (≤200 nm). The produced profile resulted in a significant contact angle decrease (from 38.7° to 5.4°). Ratios of actual surface area to projection area (r) and fraction of solid surface remaining dry (φ) were obtained from profilometry. The surface characteristics and large r values produced by EPP were able to induce *hemi-wicking*. Hence, EPP produced superhydrophilic surfaces on Ti. The bioactivity of EPP treated Ti was evaluated using cell free and MC3T3 cells *in-vitro* studies. The treated Ti surface significantly increased the bioactivity and formed stoichiometric hydroxyapatite after immersion in a bone cell culture medium for 21 days. Cells’ attachment and proliferation studies indicated that EPP treated surface significantly enhances the cells’ adhesion and growth after 24 and 48 h compared to the untreated surface. The results show that Ti surface profiling by EPP constitutes a promising method to potentially improve bone implant bonding.

Keywords

Titanium; Contact angle; Surface roughness; Hydrophilicity; Surface profile; Hydroxyapatite nucleation

[*]Corresponding author. meletis@uta.edu (E.I. Meletis).

CRediT authorship contribution statement

Wisanu Boonrawd: Conceptualization, Methodology, Validation, Investigation, Writing – original draft. **Kamal R. Awad:** Investigation, Writing – review & editing. **Venu Varanasi:** Resources, Writing – review & editing. **Efstathios I. Meletis:** Conceptualization, Resources, Supervision, Writing – review & editing.

Declaration of competing interest

The authors declare that they have no known competing financial interests or personal relationships that could have appeared to influence the work reported in this paper.

1. Introduction

Properties of materials are greatly affected by their surface characteristics such as chemistry, surface energy, and topography. Wettability of a material is the ability of a liquid droplet to spread on the surface of the material. It plays an important role in various applications ranging from anti-fogging and heat exchanging to self-cleaning and bone replacement applications. Wettability of a surface relates to its surface energy, which is a result of inherent surface chemistry and topography [1,2]. A simple way to describe wettability of a solid surface has been proposed by Young as early as 1804 [3]. Young treats contact angle (CA) of a droplet because of mechanical equilibrium of three surface tensions, as shown in Fig. 1a. Young's equilibrium equation is described by:

$$\gamma_{SV} - \gamma_{SL} = \gamma_{LV} cos\theta \quad (1)$$

where γ_{LV}, γ_{SV} and γ_{SL} are the surface tension at the interface of liquid-vapor phases, solid-vapor phases, and solid-liquid phases, respectively [4]. Later on 1936, Wenzel reported that surface roughness can affect wettability of a material [5], as described in Eq. (2)

$$cos\theta_A = rcos\theta \quad (2)$$

where r is the ratio of actual surface area to projected area, θ_A and θ are the apparent CA on a rough surface and a flat surface, respectively. Since r is always equal or greater than 1 for the textured surface, rough surface will have higher level of wettability when the chemical nature of the flat surface is hydrophilic ($\theta < 90°$). On the other hand, a rough surface can become more hydrophobic when the flat surface is naturally hydrophobic ($\theta > 90°$). The Wenzel's equation can be applied if the liquid droplet fills in the valleys of the texture. This wetting state is known as Wenzel state, as shown in Fig. 1b.

It has been reported that surfaces with proper texture can become superhydrophobic and superhydrophilic (superwetting), when water CA is larger than 150° and smaller than 10°, respectively [6–9]. However, these results are related to how the droplet spreads/sits on rough profile contours. The superhydrophobic surface state has been extensively studied due to the need for water repellant materials. Various fabrication techniques have successfully produced superhydrophobic surfaces, such as photolithography, laser texturing, and plasma processing [10]. On the other hand, literature reports on superhydrophilic surfaces are quite limited [1]. Also, superhydrophilic surface has become one of the crucial criteria for higher survival rates of the pros-thesis after implantation and shown better biological response and osseointegration [11–14]. Thus, it is worthwhile to explore new fabrication techniques to produce surface profiles that have the potential to induce desirable superwetting of surfaces.

Ti and its alloys are chemically hydrophilic in nature, thus, creating a desirable surface profile could increase wettability of the surface. Ti and its alloys have been used as bone implant materials for decades due to their excellent biocompatibility, mechanical properties, and corrosion resistance [15]. However, due to its bioinert surface, Ti cannot induce rapid bone formation and often creates fibrous tissue between the implant and the bone, which causes insufficient osseointegration [16,17]. Several studies have been focusing on surface modification of Ti to ameliorate its bioactivity, by altering surface chemistry and topography or either of them [11,18–20]. A typical way to improve Ti bioactivity is to coat hydroxyapatite (HA) on Ti surface. However, the coating layer is possible to cause implant loosening when coating delamination/detachment occurs [21–24]. This leads to an exploration of processing techniques that yield high coating adhesion strength, such as pulse laser deposition (PLD) and plasma electrolytic oxidation (PEO) [25,26]. Even though PLD is able to fabricate crystalline and high adhesion coatings, the splashing of nano-particulates on the film is the main limitation [27,28]. PEO is an emerging surface modification technique due to its ease of use and cost efficiency. However, post-heat treatment is often required to obtain crystalline phase of the HA coatings [29]. The mismatch of the coefficient of thermal expansion between the coating and the underlying substrate could result in reducing its adhesion strength [15,30,31]. Hence, more studies are focusing on altering surface topography and chemistry without introducing any coating layer [11,32–34].

Electrolytic plasma processing (EPP) is an electrochemical process operating at high electrical potential in an aqueous environment [35,36]. An energetic plasma is generated during the process and ionic species impinge on the surface of the substrate producing high surface temperatures. EPP can be conducted in two different modes, anodic or cathodic, depending on the polarity of the working electrode. The cathodic process can be used to clean and create a characteristic surface profile on the substrate in an electrolyte containing sodium hydrogen carbonate ($NaHCO_3$). Local surface melting takes place under the energetic plasma followed by quenching from the electrolyte. The local melting and freezing cycles create a characteristic “hills and valleys” profile with microroughness [36].

In this study, EPP, an environmentally friendly method, was used to create characteristic surface profiles on Ti substrates. EPP could be a necessary surface modification technique to enhance bioactivity of Ti surface. This is due to its capability to clean the surface and create unique profiles which might be able to induce superhydrophilic behavior and ameliorate bioactivity on the Ti surface. Surface characterization and bioactivity evaluation were further assisted using different techniques to clearly investigate the effect of EPP surface modification on Ti.

2. Experimental

2.1. Materials

Pure Ti (commercially pure Ti, Grade 2) discs, 0.7 cm thick and 1 cm in diameter were used as substrates. The discs were ground by silicon carbide papers down to 1000 grit as the last step and then masked to have a working surface area of about 0.8 cm^2. The samples were rinsed with acetone followed by ultrasonic cleaning in methanol for 15 min and ultrasonic cleaning in DI water for 15 min. These steps were followed for samples before and after their profiling process by EPP to eliminate oil, dirt, and contamination before performing contact angle measurements.

2.2. Electrolytic plasma processing

The electrolytic plasma process can be divided into four stages; (i) the production of fine hydrogen gas (gas liberation) due to a strong electric field from the applied potential to the electrodes, at this stage the current is increased with the applied potential. Stage (ii), scatter plasma starts to appear at the sample surface, at this stage the current drops sharply due to the breakdown of the electric field. Stage (iii), as increasing the applied potential further, the current drops to the lowest point and the plasma becomes stable and uniform. This stage is defined as working region or Kellog's region. In the last stage (iv), increasing the applied potential further, the current starts to increase again, and intense arcing is observed. Hence, the arcing is usually avoided because it causes deterioration of the surface [36,37].

Prior to EPP, the entire voltage–current density response (*V-i*) was established in a 10 wt% $NaHCO_3$ electrolyte to identify the Kellog's region, where the plasma envelope was stable. Fig. 2a represents the full *V-i* response of the setup used in this study. The current density variation was plotted *versus* the applied potential. Based on the full *V-i* response in Fig. 2a, the Kellog's region was determined to be in the range of 90–110 V with a prevailing current density of ~3 A/cm^2.

In this study, EPP was performed under the cathodic regime by controlling the input voltage using a DC power supply (SGA 600/17 DC, Sorensen, USA). A schematic drawing of the EPP system is shown in Fig. 2b. Perforated graphite was used as the counter electrode (anode). DI water containing 10 wt% of $NaHCO_3$ (99%, Alfa Aesar, USA) was used as the electrolyte with a pH 8.35. The electrolyte temperature was maintained at 75 °C. During the process, the electrolyte was circulated from a reservoir at a flow rate of 2 L/min and supplied through the perforated counter electrode onto the surface of the Ti sample. The separation distance between the counter electrode and the substrate was 5 mm. The plasma processing was conducted at 105 V for different processing times; 30 s, 60 s, 90 s, 120 s, and 150 s. Duplication samples were processed at each processing time to confirm the reproducibility of the process.

2.3. Surface characterization

2.3.1. Surface morphology and chemical composition—Scanning electron microscopy (SEM) in conjunction with energy dispersive X-ray spectroscopy (EDS) (S-3000N, Hitachi, Japan) was used to examine the surface morphology and the chemical composition of the Ti samples before and after EPP processing. The acceleration voltage during EDS analysis was kept constant at 15 kV, to minimize the excitation volume.

2.3.2. Surface profile characteristics—An optical profilometer (Wyko NT9100, Veeco Instruments Inc., USA) was used to measure the surface roughness (*Sa*) and other surface characteristics such as the average of maximum height of the hills to valleys (*Sz*), the asymmetry of surface about the mean plane (*Ssk*), and the ratio of the actual surface area to projected area (*r*). The samples were scanned at 7 different areas to cover the surface and extreme values were eliminated before determining average values.

2.3.3. Contact angle measurements—A simple sessile drop system was used to measure the CA on the Ti surface before and after the EPP profiling process. Briefly, an electronic pipet was used to drop DI water droplets, 5 μL, on the sample surface. An optical microscope was used to capture the images of the droplets on the Ti surface. Then, Adobe Photoshop was used to process the images into black and white. Finally, CA values were acquired in ImageJ software by Dropsnake analysis plugin. The CA measurements were repeated for 7 times at different locations on each sample and average values are reported.

2.4. In-vitro studies

To study the effect of Ti surface treatment on its bioactivity, cell free *in-vitro* studies were performed on the treated samples compared to the untreated Ti samples. Alpha modified minimum essential medium (α-MEM) (Gibco 12571063, USA) was used as an alternative solution to the conventional simulated body fluid (SBF) in this study [38–40]. α-MEM is an appropriate medium for bone cell culture studies; its ions concentration, pH, and amino acids and vitamins make it similar to that of human blood plasma. The ions concentration (mM) of the α-MEM are as followed Na^+ = 144.4, K^+ = 5.3, Mg^{2+} = 0.8, Ca^{2+} = 1.8, Cl^- = 126.2, HCO^{3-} = 26.2, $HPO_4^{2-} = 1.0$, $SO_4^{2-} = 0.8$ and pH = 7.4. The α-MEM has been reported to be used as an alternative SBF to evaluate HA ($Ca_{10}(PO_4)_6(OH)_2$) precipitation in *in-vitro* studies [38]. α-MEM gives similar precipitation driving forces and nucleation rates as found by Hank's balanced salt solution [39]. Untreated Ti (polished 1200 grits) samples were used as a control group. For the EPP treated samples, *in-vitro* study was performed only on the 150 s treated samples, since they exhibited the lowest contact angle. Both EPP treated and untreated Ti samples were immersed in α-MEM and kept incubated at 37 °C for 7, 14, and 21 days. The test solution was changed every 48 h to maintain ion concentration levels and pH. After completion, the samples were then rinsed with phosphate buffered saline and then dried under air environment for further characterizations.

X-ray diffraction (XRD) (D8, Bruker, USA) was used to identify the precipitation of HA. The θ-2θ scans were performed by Cu K_α radiation (λ = 1.5418 Å) with step size of 0.01° and dwell time of 3 s/step. Fourier transform infrared spectroscopy (FTIR) (Thermo Nicolet 6700 ATR, Thermo Electron Corporation, USA) was also used to confirm the presence of hydroxyl and phosphate groups in HA. Surface morphology and chemical composition were evaluated by high resolution (HR) SEM in conjunction with EDS (S-3000N and S-4800, Hitachi, Japan).

After studying the surface bioactivity using cell free media, *in-vitro* studies using murine calvarial MC3T3-E1 pre-osteoblast cells were performed to further investigate the bioactivity and the cellular behavior on the EPP treated for 150 s surface compared to the untreated Ti. All *in-vitro* studies were performed following a previous published protocol [41]. Briefly, MC3T3-E1 cells (American Type Cell Culture Inc., Manassas, VA) were cultured using α-MEM supplemented with 10% fetal bovine serum and 1% penicillin/streptomycin until 75% confluence (passage 14–15). Then, cells were seeded on the different Ti surfaces using 24 well-plates and n = 3 for each group for 24 and 48 h. After each time point, MTS assay was performed using CellTiter 96® AQueous One Solution Cell Proliferation Assay kit (Promega, Madison, WI, USA) following previously published protocol [42,43]. Briefly, MTS reagent was added directly to each well, the plate was wrapped with Al foil to be protected from the light, and the plate was incubated for 2 h. Then, the optical density (OD) readings were recorded using microplate reader (SpectraMax® i3, Molecular Devices, CA, USA) at 490 nm. Furthermore, live/dead assay using Invitrogen LIVE/DEAD Viability/Cytotoxicity Kit (Thermo Fischer Scientific Inc., Waltham, MA, USA) was performed according to previously published protocol [42]. Green stained live cells were captured as fluorescent images using a DMi8 inverted Leica microscope (Leica Microsystems Inc., IL, USA). Five images were taken for each sample and n = 3 samples for each group. Fluorescent images were further used for quantitative analysis to count the exact number of live cells on each Ti surface using ImageJ software (NIH). OriginPro 8.5 software was used for all graphs and statistical analysis, and one-way ANOVA followed by Tukey's *post hoc* was used between group comparisons. Statistical significance was considered when $p < 0.05$ represented as (*), $p < 0.01$ as (**), and (***) for $p < 0.001$.

3. Results and discussion

3.1. Chemical composition and surface morphology

EDS analysis was conducted on all EPP processed samples. Fig. 3a–b shows EDS spectra of the untreated and EPP treated Ti, respectively. The untreated Ti surface contained carbon 8.4 at.% (±1.0 at.%) and the rest was Ti. The untreated Ti surface may absorb carbon from ubiquitous hydrocarbon in air, solution containing organic contaminations, or the previous polishing process. For the EPP treated Ti, the EDS analysis revealed a small amount of carbon, 1.7 at.% (±0.5 at.%). The oxygen content on the EPP treated Ti ranged from 7 to 10 at.%. The EPP treatment eliminated surface contamination, as seen from the decreased carbon content. It's good to note that the remaining of carbon found on the EPP treated may come from the carbon residual present in the SEM chamber. Plasma processing creates a fresh and effectively clean metal surface that is highly reactive. Thus, oxygen in the air reacts with the treated Ti surface and a thin TiO_2 layer is built up. Cionea has reported that the top layer of EPP treated Ti has ultrafine grain (10–40 nm) with the depth of about 100 nm due to the repeated melting and freezing cycles during the plasma processing [44]. Thus, this thin TiO_2 layer is responsible for the small amount of oxygen content found on the EPP treated Ti. The TiO_2 is capable of forming hydroxyl groups on its surface, which may help decreasing the contact angle of water droplets [45].

Scanning electron micrographs of the EPP profiled Ti at different processing time are shown in Fig. 4. Characteristic hills, valleys, and crater-like features appear across the surface of the EPP profiled Ti. These features were a result of local surface melting by high temperature discharge created by EPP. Then, the collapse of high energetic plasma at the vicinity of the titanium surface produced shock waves. Subsequently, fast solidification takes place due to the presence of aqueous electrolyte [35,36]. Elias et al. and Le Guéhennec et al. have reported that crater-like and pore features on the surface exhibit higher wettability and removal torque after *in-vitro* and *in-vivo* tests, compared to other rough surfaces without these features [13,24]. The removal torque is a measurement used to assess biomechanical anchorage or endosseous integration. A high surface removal torque implies good bone integration with the substrate material.

The SEM images also reveal that the size and number of crater-like features were increased by increasing processing time. The processed surfaces exhibited complex texture such as protruding and undercutting features for plasma processing at or longer than 90 s. These features are greatly increasing the surface area of the EPP profiled Ti. Furthermore, there were submicrometer (80–350 nm in diameter) pores embedded in the protruding features. The high surface area and the presence of pores can increase the wettability of the surface by letting the liquid droplet imbibe through those pores. Thus, the wetting state may not solely follow the Wenzel state, where the surface is dry ahead of the contact line, but rather exhibiting film state, where the texture is filled with a liquid film [46]. The condition for droplet imbibition will be discussed in the following section.

3.2. Wettability and surface roughness

The wettability of the surface was investigated by CA measurements. An example of a water droplet on an untreated and plasma processed Ti surface is shown in Fig. 5a and b, respectively. The CA variation of the Ti samples at different processing times is shown in Fig. 6a. The CA for the unprocessed sample (denoted as 0 s) is also included for comparison. The results revealed that the untreated Ti was hydrophilic with a CA of 38.7°. After plasma processing, the CA decreased significantly (~82%) exhibiting only a small decrease with increasing processing time. It is important to note that even an EPP treatment for 30 s produced a surface profile, Fig. 4b, with a very low CA (~9°). Thus, the wettability of the Ti samples was increased and became superhydrophilic after subjected to EPP profiling. The highest wettability (average AC of 5.4°) was observed for the profile produced after 150 s of processing, Fig. 4f.

The results of *Sa* and *Sz versus* processing time are shown in Fig. 6b–c, respectively. *Sa* is the measurement of surface roughness in 3D while *Sz* is the measurement of surface maximum height from the top of the hill to the bottom of the valley. The profilometer is taking the average of 5 maximum values for a specific scanned area. The results clearly show that increasing processing time resulted in an increase in roughness parameters. The trend of the increase of *Sa* is almost linear since longer processing time allows plasma processing to produce rough characteristic surface from numerous cycles of local melting and freezing events. Even a 30 s treatment produces a significant increase in *Sa* from 17 nm for the untreated surface to 87 nm. The highest surface roughness was achieved after processing for 150 s exhibiting a value of *Sa* 213 nm. It is important to note that the EPP treatment produced a nanoscale roughness with the *Sa* parameter remaining at or below ~200 nm for all treatments. Gui et al. performed EPP treatment (cleaning) on 304 stainless steel at different processing time and found a similar trend for the surface roughness, even though it has been analyzed in 2D (*Ra*) [47].

The results of *Sz* present the average variation of the distance between the top of the hill and bottom of the valley features with processing time. The trend of *Sz* with processing time exhibits a sharp increase initially and more of a plateau after 60 s. Furthermore, initially the variation was obviously high which was probably due to insufficient processing for such short duration. Beyond 60 s of treatment, *Sz* seems to stabilize at about 3 μm. Another surface roughness parameter obtained is *Ssk* that is used to evaluate the profile symmetry of the surface about the mean plane. The value of the *Ssk* can be negative, zero, or positive. The negative skew means the bulk of the material is above the mean plane where the positive skew is the opposite. This implies that the negative skew surface mostly comprises deep valleys rather than spikes. The zero skew means the surface is more symmetric [48]. In this study, the untreated sample had a negative skew as seen from the results in Fig. 6d. This is a result of the presence of scratches from the mechanical grinding process. However, the negative skewness has reduced after subjected to the EPP profiling, moreover, it became closer to zero after EPP profiling for 90 s and longer. This is due to the effect by the fine plasma during EPP producing a profile with higher *Ssk* uniformity. Thus, the EPP has created a new texture on the Ti surface with comparatively equal amounts of spikes and valleys. Furthermore, the results revealed that a type of hierarchical profile was produced composed of ~3 μm spikes (2 μm < *Sz* < 3 μm) separate by valleys with nanoscale roughness (100 nm < *Sa* < 200 nm).

3.3. Superhydrophilicity of EPP profiled surfaces

Prior to discussing how superhydrophilicity was induced on EPP profiled surfaces, it is beneficial to give a brief explanation on how superhydrophobic surface is developed since it is the opposite phenomenon. A textured solid surface can become superhydrophobic when the liquid droplet rests between spikes or protrusions. Air must be trapped in the cavities under the liquid droplet. This follows the Cassie-Baxter wetting state as shown in Fig. 5c [49]. However, the trapping of air is metastable since the liquid droplet will eventually wet the solid surface in the cavity, transition to Wenzel state, due to lower energy state of their interactions. Bico et al. [46] applied Young’s and Wenzel’s equations and reported that the condition for the stability of the liquid droplet on air cavities followed Eq. (3):

$$cos\theta < \frac{\varphi - 1}{r - \varphi} \tag{3}$$

where θ, r, and φ are Young’s contact angle on flat surface, the ratio of the actual surface area to the projected one, and the fraction of solid surface remaining dry, respectively.

For the superhydrophilic case, the liquid drop must be *hemi-wicking*, which is the opposite to the pinning of the droplet for the case of superhydrophobic. *Hemi-wicking* is the mechanism that the liquid droplet is intermediate between imbibition and spreading into the cavities of the textured surface. This wetting state has been proposed as film state. Fig. 5d is the schematic drawing of a liquid droplet on a textured surface representing the film wetting state. Hence, this gives the prerequisite conditions for superhydrophilic surface as follows [46,50]:

$$cos\theta > \frac{1 - \varphi}{r - \varphi}, \quad \theta < \theta_c \quad \text{with} \quad cos\theta_c = \frac{1 - \varphi}{r - \varphi} \tag{4}$$

where θ_c is the critical contact angle.

Table 1 presents the r and φ measurements for all EPP processed samples. The surface profiling results revealed that the r value increased significantly by increasing processing time in the EPP profiling process. The untreated sample had an r value of 1.1, then increased to 12.4 after subjected to EPP profiling process for only 30 s. Moreover, the r value went up to 88.6 after processing for 150 s. This was consistent with the *Sa* and *Sz* results, since rougher surfaces provided larger surface area [51]. In view of Eq. (4), when r is comparatively large, the condition for *hemi-wicking* is favored. Thus, the surface of Ti has turned to superhydrophilic after the EPP profiling process.

Representative contour spectral and 2D surface line profiles as a function of treatment time are shown in Fig. 7. They were used to evaluate and calculate the φ values. As seen from the SEM images in Fig. 4, the geometry on top of the features of the EPP profiled surface was nonuniform since the protrusions were randomly created by the collapse of the plasma. The contour spectral images are representing the distribution of the height over the scanned area. They show that for the clear majority of hills, their height on the profiled surface is at least in the range of about 0.4 μm. In view of Eq. (4), in a surface with a high value of r ($r > 5$) and naturally hydrophilic (apparent contact angle $\theta < 75°$), water droplets will imbibe and spread to fill up between these protrusions and valleys. This results in wetting of the surface regardless of φ values. The summation of the area on top of each spike above the droplets is the φ value. However, the EPP produced features with a variation in height and it is hard to precisely calculate their surface area on the tip of them. Thus, the portion of spikes at and above 0.4 μm was considered as the surface remaining dry since most asperities and valleys are lying below them. The cross-sectional areas at the height of 0.4 μm and above will be representing the surface remaining dry area of the asperities. These areas appear in saturated red in the contour spectral images of Fig. 7. ImageJ software was used to determine the sum of the areas in saturated red and extract the φ values that are reported in Table 1. The EPP profiled samples had φ values of 3.1%, 3.6%, 4.1%, 4.2% and 4.6% after processing for 30 s, 60 s, 90 s, 120 s and 150 s, respectively. The 2D surface line results provided additional evidence that the longer processing time produces a higher number of tall spikes and deep valleys. It is important to note that the proposed criterion for surface remaining dry could possibly overestimate the φ values. Nevertheless, these surfaces have sufficiently large r ($r >$ 12) and their apparent contact angle on flat surface is small enough ($\theta = 38.7°$) to be able to neglect possible overestimation of φ values.

Fig. 8 present the distribution of the area of the solid surface remaining dry for each processing time. The results clearly show that prolonging processing time produced a larger number of smaller size spikes scattered across the surface. The increase in number of small spikes results in a substantial increase in r, which is favorable for inducing the *hemi-wicking* mechanism and, finally, lower CA of the droplets. In superhydrophilic and superhydrophobic surface design, line density (*i.e.*, spike or hill density) and asperity height are one of the most important parameters to be considered [52]. The line density in the present study can be determined by dividing the scanned area shown in Fig. 7 with the total number of spikes taller than 4 μm from Fig. 8. For example, for a 150 s treatment, the results show that there is a spike taller than 0.4 μm in every 10 μm^2 of the profiled surface. Such a combination of spike line density and height is expected to be beneficial for the spread of droplets [53].

The critical CAs for the processed samples were calculated following Eq. (4). The apparent and critical CA for each processing time were plotted and shown in Fig. 5e. As mentioned above, when the critical CA is larger than the apparent contact angle, superhydrophilicity will be achieved as a result of the *hemi-wicking*. It can be seen that the surface condition of the untreated sample yielded a critical CA of 24.0° which was smaller than the apparent

CA, 38.6°. Thus, it was not able to induce superwetting of the surface. However, after EPP profiling, the surfaces yielded critical CA values close to 90°. In other words, the textured created by EPP profiling was able to induce superhydrophilicity on the titanium surface.

Thus far in this section, superwetting mechanism of the EPP treated surface has been discussed based on its topography. Our findings showed that wettability mainly depends on *Sz* and *Ssk* (both exhibiting a small increase with processing time) and not much on *Sa* (increase in roughness). Another factor affecting wettability is the surface chemistry. As mentioned earlier, the EPP produced clean surface with a thin TiO_2 layer for all treated samples including the one processed for 30 s. The TiO_2 has been reported to be able to form hydroxyl groups, which may help decreasing the contact angle. However, this would happen when TiO_2 reacts with a liquid at physiological pH values and a certain thickness may be required [45]. Also, the EPP treated samples showed an insignificant amount of carbon contamination on their surface. It is known that a surface with less contamination possesses higher surface free energy [54,55]. Hence, it is readily to reduce its surface free energy by bonding with the water droplets that land on its surface. In addition, the EPP profiling surfaces have such large r value that satisfying *hemi-wicking* mechanism. It can be concluded that the combinations of surface chemistry and topography yield superwetting characteristic on the EPP treated Ti surface.

It is important to note that the EPP profiled samples were not able to achieve complete wetting (*i.e.*, CA of 0°). It is noted that Wenzel's equation suggests that rough surface satisfying $\cos\theta > 1 / r$, corresponding to $dE < 0$ can exhibit complete wetting [53,56]. However, this is not accomplished since the real surface can not completely imbibe the liquid droplet. In addition, superhydrophilic surface is sensitive to contamination as a result of its high surface energy. By exposing the surface to air environment, contamination from airborne can easily reduce the wettability of the surface [1,57]. Nevertheless, the present results show that EPP is a promising profiling method to induce superhydrophilicity on titanium surfaces. This is particularly important for titanium and its alloys since they are biocompatible and widely used materials for biomedical applications.

3.4. In-vitro study

3.4.1. Cell free studies—HR-SEM images, Fig. 9, represent the surface morphologies of Ti samples after immersion in α-MEM for 7, 14, and 21 days. It is clearly seen that both treated and untreated groups were able to induce calcium phosphate nucleation on their surface after 7 days of immersion. This is due to the α-MEM is metastable and supersaturated towards calcium phosphate crystals. It will eventually reduce its energy by forming calcium phosphate crystals when the time and temperature are suitable [58]. However, it can be clearly seen that the EPP treated Ti surface showed a higher density of calcium phosphate deposition compared to that of the control group. The EPP treated Ti has better hydrophilicity level and larger surface area due to its rougher profile compared to the untreated Ti. An increase of material surface area can lead to better protein adsorption and faster change of local α-MEM composition, thus, a faster calcium phosphate crystal formed on the surface [58,59]. Moreover, a solid surface with high surface energy will provide a better nucleation site for heterogeneous nucleation. Since its interfacial energy with calcium phosphate-nucleus is lower than that of nucleus-solution interface. Hence, calcium phosphate nucleates and grows faster on the EPP treated Ti in α-MEM. The results of apatite coverage analyzed in ImageJ software, shown in Fig. 10a–g, provide additional evidence that the EPP treated Ti surface has higher nucleation rate as we can see from the percentage of apatite coverage. At day 7, the apatite coverage of the untreated and EPP treated Ti was at 18.7% (±2.1%) and 35.0% (±2.6%), respectively. After immersion for 21 days, the apatite coverage increased to 33.0% (±3.0%) and 72.3% (±2.1%) for the untreated and EPP treated Ti, respectively. Saruta et al. has reported similar results from their study on osteoconductive of acid etched Ti that has surface features close to that found on EPP treated Ti for 150 s [60]. They found that the Ti with sub-micro-scale topography, having pit size in the range of 0.1–0.5 μm, had better calcium deposition and expression of osteoblastic compared to the group without such compartmental structure. Furthermore, there has also been reported that Ti with surface texture prepared by various techniques, such as blasting, selective laser melting and anodic oxidation, exhibit better osteoconductive/osteointegration compared to flat surface [19,55,61]. Thus, it is important to note that surface topography and hydrophilicity play an important role on bioactivity level of Ti implants.

EDS analysis showed that Ca/P ratio increased with increasing immersion time. The Ca/P ratio of the EPP treated Ti after immersed in α-MEM for 7, 14 and 21 days was 1.33 (±0.08), 1.47 (±0.05) and 1.68 (±0.02), respectively. Fig. 10h represents the Ca/P atomic ratio of the stoichiometric HA and the EPP treated Ti as a function of the immersion time in α-MEM. At early stage, octacalcium phosphate (OCP, stoichiometric Ca/P ratio = 1.33), was formed after immersion in α-MEM for 7 days. This was in a good agreement to the results that Awad et al. found when immersed Ti6Al4V alloy in α-MEM for 7 days [38]. The OCP morphologies are shown in Fig. 9a–f. As immersion continued, the plate like morphology of OCP precipitation has developed to dense tricalcium phosphate (TCP, stoichiometric Ca/P ratio = 1.50) after immersed in α-MEM for 14 days. Wang et al. also reported that at early stage of *in vivo* implantation dicalcium phosphate, OCP and TCP tend to form before HA [62]. It is worth mentioning that OCP and TCP are thermodynamically metastable phases, the formation of them at early stage is kinetically favored. Eventually, HA (stoichiometric Ca/P ratio = 1.67) was found after immersion in α-MEM for 21 days. The formation of HA is probably due to the hydrolysis of OCP as shown in Eq. (5) [63].

$$Ca_8H_2(PO_4)_6 \cdot 5H_2O + 2Ca^{2+} \rightarrow Ca_{10}(PO_4)_6(OH)_2 + 4H^+ \quad (5)$$

HA is the most stable form of calcium phosphate in physiological environment. It has been reported that HA is able to bond better with surrounding bone rather than dissolve like other unstable calcium phosphate phases *in-vivo* [62,63].

FTIR spectrum of EPP treated Ti after immersion in α-MEM for 21 days, Fig. 11a, is the evidence that HA has precipitated on the surface. The FTIR spectrum is similar to that of HA powders reported by other studies [64–66]. The absorption peaks of PO_4^{3-} at 900–1200 and 570 cm^{-1} are attributed to the formation of HA. The shoulder peaks at 3560, 2800, and 600 cm^{-1} are due to the OH stretching of HA. XRD results also confirmed the formation of HA with the presence of HA (211) and HA (203) peaks at $2\theta = 31.77°$ and 45.31°, respectively (JCPDS #09-0432). The XRD pattern of EPP treated Ti after immersion in α-MEM for 21 days is shown in Fig. 11b. It is important to note that the SBF or α-MEM is not able to mimic the ability of living physiological system, *i.e.*, maintaining stable range of pH level over time. However, at present both solutions provide a useful tool to predict the bioactivity of a material before its implantation *in-vivo* [67].

3.4.2. MC3T3 cell culture studies—*In-vitro* cell culture studies were performed to evaluate the cells' attachment, proliferation, and viability on the EPP treated Ti surface. Fig. 12a–d presents fluorescent images of live cell (green) attachment and growth on the Ti surfaces. It can be clearly noticed that the cell attachment and viability are significantly higher on the EPP treated Ti surfaces, *i.e.*, Fig. 12b and d compared to the untreated surface Fig. 12a and c after immersion for 24 and 48 h, respectively. For quantitative analysis, the fluorescence images were further used to count the exact number of cells on each sample and the data are presented as box plots in Fig. 12e. The number of cells was significantly higher on EPP treated surface (236 ± 45 and 362 ± 80, at 24 and 48 h, respectively) compared to the untreated surface (176 ± 39 and 244 ± 74, at 24 and 48 h, respectively) with a significance degree of ***$p < 0.001$. Furthermore, MTS assay was used for quantitative analysis of the cells' proliferation and growth after 24 and 48 h as indicated in Fig. 12f. The MTS assay findings confirmed the results obtained from the live cell's count indicating a higher cell's attachment and proliferation on the EPP treated surface compared to the untreated Ti surface. Tissue culture plate was used as a positive control for the MTS study. It is important to note that there was no significant difference in the cell's viability between the EPP treated Ti surface compared to the positive control. While both positive control and EPP treated surfaces were significantly higher in the cell's viability compared to the untreated surface at 24 and 48 h with a significance degree of *$p < 0.05$ and **$p < 0.01$. From these data it is concluded that the EPP treated surface could enhance the cells' viability and proliferation without any cytotoxicity effects.

4. Conclusions

Electrolytic plasma processing of Ti produced a characteristic hierarchical surface profile comprised of 2–3 μm size hills and valleys exhibiting nanoscale roughness. The roughness increased with processing time, but it remained below 200 nm. Analysis of EPP profile parameters showed the development of several beneficial profile characteristics including a major increase in the ratio of the actual surface area to projection area. The EPP produced profile resulted in high critical contact angle values inducing *hemi-wicking* and significant reduction in the droplet contact angle. The EPP treatment was able to produce desirable profile characteristics on pure Ti surface resulting in superhydrophilic behavior. Furthermore, its superhydrophilic surface was able to induce HA formation after immersed in an alternative SBF (α-MEM) for 21 days. *In-vitro* cell culture studies using MC3T3 pre-osteoblast cells indicated the significant enhancement in the cells' viability and proliferation on the EPP treated Ti surface compared to the untreated Ti. Thus, superhydrophilicity of the Ti surface can increase the precipitation rate of calcium phosphate-based compounds that are related to the mineral phase of bone.

Acknowledgment

The authors would like to acknowledge Dr. Randall Kelton for his advice on contact angle measurement set up and image processing. Analysis of the samples was conducted at the Characterization Center for Materials & Biology and the Bone-Muscle Research Center at the University of Texas at Arlington.

References

[1]. Drelich J, Chibowski E, Meng DD, Terpilowski K, Hydrophilic and superhydrophilic surfaces and materials, Soft Matter 7 (2011) 9804–9828, 10.1039/c1sm05849e.

[2]. Jennissen HP, Hyperhydrophilic rough surfaces and imaginary contact angles, Materwiss, Werksttech. 43 (2012) 743–750, 10.1002/mawe.201200961.

[3]. Young T, An essay on the cohesion of fluids, Philos, Trans. R. Soc. Lond 95 (1804) 65–87, 10.1098/rstl.1805.0005.

[4]. Zisman WA, Relation of the equilibrium contact angle to liquid and solid constitution, in: Gould RF (Ed.), Contact Angle, Wettability, Adhes, American Chemical Society, Washington, DC, 1964, pp. 1–51, 10.1021/ba-1964-0043.ch001.

[5]. Wenzel RN, Resistance of solid surfaces to wetting by water, Ind, Eng. Chem 28 (1936) 988–994, 10.1021/ie50320a024.

[6]. Gatapova EY, Semenov AA, Zaitsev DV, Kabov OA, Evaporation of a sessile water drop on a heated surface with controlled wettability, Colloids Surf, A Physicochem. Eng. Asp 441 (2014) 776–785, 10.1016/j.colsurfa.2013.05.046.

[7]. Shibuichi S, Onda T, Satoh N, Tsujii K, Super water-repellent surfaces resulting from fractal structure, J. Phys. Chem 100 (1996) 19512–19517, 10.1021/jp9616728.

[8]. Roach P, Shirtcliffe NJ, Newton MI, Progess in superhydrophobic surface development, Soft Matter 4 (2008) 224–240, 10.1039/b712575p. [PubMed: 32907233]

[9]. Fleming RA, Zou M, Silica nanoparticle-based films on titanium substrates with long-term superhydrophilic and superhydrophobic stability, Appl, Surf. Sci 280 (2013) 820–827, 10.1016/j.apsusc.2013.05.068.

[10]. Liu X, Liang Y, Zhou F, Liu W, Extreme wettability and tunable adhesion: biomimicking beyond nature? Soft Matter 8 (2012) 2070–2086, 10.1039/c1sm07003g.

[11]. Wennerberg A, Jimbo R, Stübinger S, Obrecht M, Dard M, Berner S, Nanostructures and hydrophilicity influence osseointegration: a biomechanical study in the rabbit tibia, Clin, Oral Implants Res. 25 (2014) 1041–1050, 10.1111/clr.12213. [PubMed: 23782316]

[12]. Jorge MZ, Granjeiro JM, Sartoretto SC, Calasans-Maia MD, Alves ATNN, Zarranz L, Hydrophilic surface of Ti6Al4V-ELI alloy improves the early bone apposition of sheep tibia, Clin, Oral Implants Res. 28 (2016) 893–901, 10.1111/clr.12894. [PubMed: 27317626]

[13]. Elias CN, Oshida Y, Lima JHC, Muller CA, Relationship between surface properties (roughness, wettability and morphology) of titanium and dental implant removal torque, J. Mech. Behav. Biomed. Mater 1 (2008) 234–242, 10.1016/j.jmbbm.2007.12.002. [PubMed: 19627788]

[14]. Hotchkiss KM, Reddy GB, Hyzy SL, Schwartz Z, Boyan BD, Olivares-Navarrete R, Titanium surface characteristics, including topography and wettability, alter macrophage activation, Acta Biomater. 31 (2016) 425–434, 10.1016/j.actbio.2015.12.003. [PubMed: 26675126]

[15]. Liu X, Chu PK, Ding C, Surface modification of titanium, titanium alloys, and related materials for biomedical applications, Mater. Sci. Eng. R Reports 47 (2004) 49–121, 10.1016/j.mser.2004.11.001.

[16]. Vijayaraghavan V, Sabane AV, Tejas K, Hypersensitivity to titanium: a less explored area of research, J. Indian Prosthodont. Soc 12 (2012) 201–207, 10.1007/s13191-012-0139-4. [PubMed: 24293916]

[17]. Bosshardt DD, Chappuis V, Buser D, Osseointegration of titanium, titanium alloy and zirconia dental implants: current knowledge and open questions, Periodontol. 2000. 73 (2017) 22–40. doi:10.1111/prd.12179.

[18]. Cooper LF, A role for surface topography in creating and maintaining bone at titanium endosseous implants, J. Prosthet. Dent 84 (2000) 522–534, 10.1067/mpr.2000.111966. [PubMed: 11105008]

[19]. Schwarz MLR, Kowarsch M, Rose S, Becker K, Jani L, Jani L, Effect of surface roughness, porosity, and a resorbable calcium phosphate coating on osseointegration of titanium in a minipig model, J. Biomed. Mater. Res. Part A 89A (2008) 667–678, 10.1002/jbm.a.32000.

[20]. Liu Y, Wang J, Chen X, Deng F, Zhang C, Xu J, Improved bioactivity of selective laser melting titanium: surface modification with micro-/nano-textured hierarchical topography and bone regeneration performance evaluation, Mater. Sci. Eng. C 68 (2016) 229–240, 10.1016/j.msec.2016.05.096.

[21]. Chang YL, Lew D, Park JB, Keller JC, Biomechanical and morphometric analysis of hydroxyapatite-coated implants with varying crystallinity, J. Oral Maxillofac. Surg 57 (1999) 1096–1108, 10.1016/S0278-2391(99)90333-6. [PubMed: 10484111]

[22]. Lee JJ, Rouhfar L, Beirne OR, Survival of hydroxyapatite-coated implants: a meta-analytic review, J. Oral Maxillofac. Surg 58 (2000) 1372–1379, 10.1053/joms.2000.18269. [PubMed: 11117685]

[23]. Tinsley D, Watson CJ, Russell JL, A comparison of hydroxylapatite coated implant retained fixed and removable mandibular prostheses over 4 to 6 years, Clin, Oral Implants Res 12 (2001) 159–166, 10.1034/j.1600-0501.2001.012002159.x. [PubMed: 11251666]

[24]. Le Guéhennec L, Soueidan A, Layrolle P, Amouriq Y, Surface treatments of titanium dental implants for rapid osseointegration, Dent, Mater. 23 (2007) 844–854, 10.1016/j.dental.2006.06.025. [PubMed: 16904738]

[25]. Rokosz K, Hryniewicz T, Matýsek Dudek D, Valíček J, Harničárová M, SEM and EDS analysis of surface layer formed on titanium after plasma electrolytic oxidation in H_3PO_4 with the addition of $Cu(NO_3)_2$, J. Nanosci. Nanotechnol 16 (2016) 7814–7817, 10.1166/jnn.2016.12558.

[26]. Rokosz K, Hryniewicz T, Malorny W, Characterization of porous coatings obtained on materials by plasma electrolytic oxidation, Mater. Sci. Forum 862 (2016) 86–95, 10.4028/www.scientific.net/MSF.862.86.

[27]. Cheung J, Horwitz J, Pulsed laser deposition history and laser-target interactions, MRS Bull. (1992) 30–36, 10.1557/S0883769400040598.

[28]. Eliaz N, Metoki N, Calcium phosphate bioceramics: a review of their history, structure, properties, coating technologies and biomedical applications, Materials. 10 (2017) 334, 10.3390/ma10040334.

[29]. Rafieerad AR, Ashra MR, Mahmoodian R, Bushroa AR, Surface characterization and corrosion behavior of calcium phosphate-base composite layer on titanium and its alloys via plasma electrolytic oxidation: a review paper, Mater. Sci. Eng. C 57 (2015) 397–413, 10.1016/j.msec.2015.07.058.

[30]. Mohseni E, Zalnezhad E, Bushroa AR, Comparative investigation on the adhesion of hydroxyapatite coating on Ti-6Al-4V implant: a review paper, Int, J. Adhes. Adhes 48 (2014) 238–257, 10.1016/j.ijadhadh.2013.09.030.

[31]. Rats D, Vandenbulcke L, Herbin R, Benoit R, Erre R, Serin V, Sevely J, Characterization of diamond films deposited on titanium and its alloys, Thin Solid Films 270 (1995) 177–183, 10.1016/0040-6090(95)06913-5.

[32]. Arola DD, McCain ML, Abrasive waterjet peening: a new method of surface preparation for metal orthopedic implants, J. Biomed. Mater. Res 53 (2000) 536–546, 10.1002/1097-4636(200009)53:5<536::AID-JBM13>3.0.CO;2-V. [PubMed: 10984702]

[33]. Ozdemir Z, Ozdemir A, Basim GB, Application of chemical mechanical polishing process on titanium based implants, Mater. Sci. Eng. C 68 (2016) 383–396, 10.1016/j.msec.2016.06.002.

[34]. Trisi P, Marcato C, Todisco M, Bone-to-implant apposition with machined and MTX microtextured implant surfaces in human sinus grafts., Int, J. Periodontics Restorative Dent 23 (2003) 427–437, 10.11607/prd.00.0547. [PubMed: 14620117]

[35]. Smith A, Kelton R, Meletis EI, Deposition of Ni coatings by electrolytic plasma processing, Plasma Chem. Plasma Process 35 (2015) 963–978, 10.1007/s11090-015-9642-9.

[36]. Meletis EI, Nie X, Wang FL, Jiang JC, Electrolytic plasma processing for cleaning and metal-coating of steel surfaces, Surf, Coat. Technol 150 (2002) 246–256, 10.1016/S0257-8972(01)01521-3.

[37]. Yerokhin A, Pilkington A, Matthews A, Pulse current plasma assisted electrolytic cleaning of AISI 4340 steel, J. Mater. Process. Technol 210 (2010) 54–63, 10.1016/j.jmatprotec.2009.08.018.

[38]. Awad KR, Ahuja N, Shah A, Tran H, Aswath PB, Brotto M, Varanasi V, Silicon nitride enhances osteoprogenitor cell growth and differentiation via increased surface energy and formation of amide and nanocrystalline HA for craniofacial reconstruction, Med, Devices Sens. 2 (2019), e10032, 10.1002/mds3.10032.

[39]. Lee JTY, Leng Y, Chow KL, Ren F, Ge X, Wang K, Lu X, Cell culture medium as an alternative to conventional simulated body fluid, Acta Biomater. 7 (2011) 2615–2622, 10.1016/j.actbio.2011.02.034. [PubMed: 21356333]

[40]. Bohner M, Lemaitre J, Can bioactivity be tested in vitro with SBF solution? Biomaterials. 30 (2009) 2175–2179, 10.1016/j.biomaterials.2009.01.008. [PubMed: 19176246]

[41]. Ahuja N, Awad KR, Brotto M, Aswath PB, Varanasi V, A comparative study on silicon nitride, titanium, and poly-ether ether ketone on mouse pre-osteoblasts cells, Med, Devices Sens. n/a (2020), e10139, 10.1002/mds3.10139.

[42]. Awad K, Ahuja N, Fiedler M, Peper S, Wang Z, Aswath P, Brotto M, Varanasi V, Ionic silicon protects oxidative damage and promotes skeletal muscle cell regeneration, Int. J. Mol. Sci 22 (2021) 497, 10.3390/ijms22020497.

[43]. do Monte FA, Ahuja N, Awad KR, Pan Z, Young S, Kim HKW, Aswath P, Brotto M, Varanasi VG, Silicon oxynitrophosphide nanoscale-coating enhances antioxidant marker -induced angiogenesis during in vivo cranial bone defect healing, JBMR Plus. n/a (2020), e10425, 10.1002/jbm4.10425.

[44]. Cionea C, Microstructualral Evolution of Surface Layers During Electrolytic Plasma Processing, The University of Texas at Arlington, 2010.

[45]. Jennissen HP, Ultra-hydrophilic transition metals as histophilic biomaterials, Macromol, Symp. 225 (2005) 43–69, 10.1002/masy.200550705.

[46]. Bico J, Tordeux C, Qúeŕe D, Rough wetting, Europhys, Lett. 55 (2001) 214–220, 10.1209/epl/i2001-00402-x.

[47]. Gui W, Lin J, Hao G, Qu Y, Liang Y, Zhang H, Electrolytic plasma processing-an innovative treatment for surface modification of 304 stainless steel, Sci, Rep. 7 (2017) 1–7, 10.1038/s41598-017-00204-w. [PubMed: 28127051]

[48]. Leach R, Characterisation of Areal Surface Texture, Springer, London, 2013, 10.1007/978-3-642-36458-7.

[49]. Cassie ABD, Baxter S, Wettability of porous surfaces, Trans, Faraday Soc. 40 (1944) 546–551, 10.1039/tf9444000546.

[50]. Kim BS, Shin S, Shin SJ, Kim KM, Cho HH, Control of superhydrophilicity/superhydrophobicity using silicon nanowires via electroless etching method and fluorine carbon coatings, Langmuir. 27 (2011) 10148–10156, 10.1021/la200940j. [PubMed: 21728376]

[51]. Xu S, Hartvickson S, Zhao JX, Increasing surface area of silica nanoparticles with a rough surface, ACS Appl. Mater. Interfaces 3 (2011) 1865–1872, 10.1021/am200052a. [PubMed: 21561089]

[52]. Extrand CW, Criteria for ultralyophobic surfaces, Langmuir. 20 (2004) 5013–5018, 10.1021/la036481s. [PubMed: 15984262]

[53]. Otitoju TA, Ahmad AL, Ooi BS, Superhydrophilic (superwetting) surfaces: a review on fabrication and application, J. Ind. Eng. Chem 47 (2017) 19–40, 10.1016/j.jiec.2016.12.016.

[54]. Pratap T, Patra K, Fabrication of micro-textured surfaces using ball-end micromilling for wettability enhancement of Ti-6Al-4V, J. Mater. Process. Technol 262 (2018) 168–181, 10.1016/j.jmatprotec.2018.06.035.

[55]. Zhu X, Reichl R, Geis-Gerstorfer J, Chen J, Scheideler L, Effects of topography and composition of titanium surface oxides on osteoblast responses, Biomaterials. 25 (2003) 4087–4103, 10.1016/j.biomaterials.2003.11.011.

[56]. McHale G, Shirtcliffe NJ, Aqil S, Perry CC, Newton MI, Topography driven spreading, Phys. Rev. Lett 93 (2004) 036102 1–4. doi:10.1103/PhysRevLett.93.036102.

[57]. Fleming RA, Zou M, Fabrication of stable superhydrophilic surfaces on titanium substrates, J. Adhes. Sci. Technol 28 (2014) 823–832, 10.1080/01694243.2012.697754.

[58]. Lu X, Leng Y, Theoretical analysis of calcium phosphate precipitation in simulated body fluid, Biomaterials. 26 (2005) 1097–1108, 10.1016/j.biomaterials.2004.05.034. [PubMed: 15451629]

[59]. Schmidt DR, Waldeck H, Kao WJ, Protein adsorption to biomaterials, in: Puleo DA, Bizios R (Eds.), Biol. Interact. Mater. Surfaces Underst. Control. Protein, Cell, Tissue Responses, Spring, New York, 2009.

[60]. Saruta J, Sato N, Ishijima M, Okubo T, Hirota M, Ogawa T, Disproportionate effect of sub-micron topography on osteoconductive capability of titanium, Int. J. Mol. Sci 20 (2019), 4027, 10.3390/ijms20164027 (1–15).

[61]. Shah FA, Grandfield K, Palmquist A, 9 - laser surface modification and the tissue-implant interface, in: Vilar R (Ed.), Laser Surf. Modif. Biomater. Tech. Appl, Elsevier Ltd, New York, 2016. doi:10.1016/B978-0-08-100883-6.00009-5.

[62]. Wang H, Eliaz N, Xiang Z, Hsu HP, Spector M, Hobbs LW, Early bone apposition in vivo on plasma-sprayed and electrochemically deposited hydroxyapatite coatings on titanium alloy, Biomaterials. 27 (2006) 4192–4203, 10.1016/j.biomaterials.2006.03.034. [PubMed: 16618502]

[63]. Wang L, Nancollas GH, Calcium orthophosphates: crystallization and dissolution, Chem. Rev 108 (2008) 4628–4669, 10.1021/cr0782574. [PubMed: 18816145]

[64]. Gheisari H, Karamian E, Abdellahi M, A novel hydroxyapatite -Hardystonite nanocomposite ceramic, Ceram. Int 41 (2015) 5967–5975, 10.1016/j.ceramint.2015.01.033.

[65]. Junker R, Dimakis A, Thoneick M, Jansen JA, Effects of implant surface coatings and composition on bone integration: a systematic review, Clin, Oral Implants Res. 20 (2009) 185–206, 10.1111/j.1600-0501.2009.01777.x. [PubMed: 19663965]

[66]. Nie X, Leyland A, Matthews A, Deposition of layered bioceramic hydroxyapatite/TiO2 coatings on titanium alloys using a hybrid technique of micro-arc oxidation and electrophoresis, Surf, Coat. Technol 125 (2000) 407–414, 10.1016/S0257-8972(99)00612-X.

[67]. Kokubo T, Takadama H, How useful is SBF in predicting in vivo bone bioactivity? Biomaterials. 27 (2006) 2907–2915, 10.1016/j.biomaterials.2006.01.017. [PubMed: 16448693]

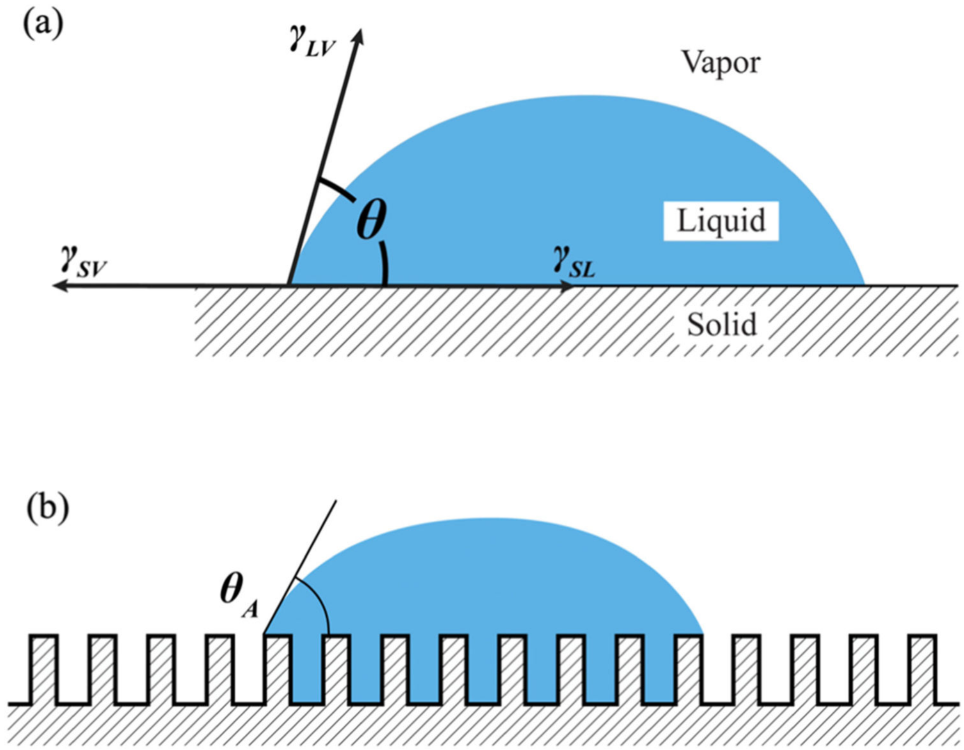

Fig. 1.
(a) Young's equilibrium contact angle and (b) Wenzel wetting state of a rough surface.

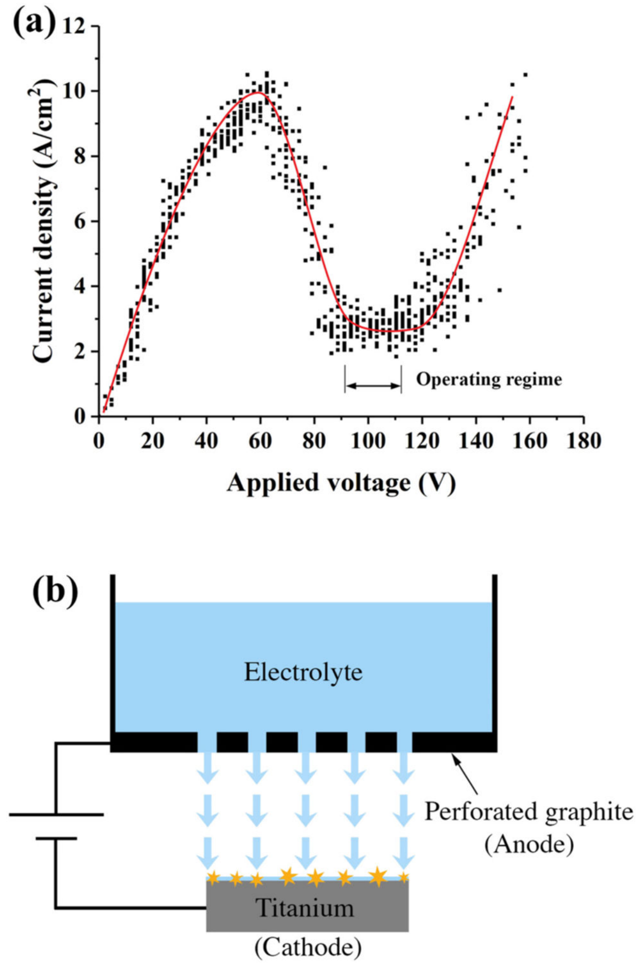

Fig. 2.

(a) Full EPP *V-i* response of pure titanium in 10 wt% $NaHCO_3$ and (b) schematic drawing of the electrolytic plasma processing unit.

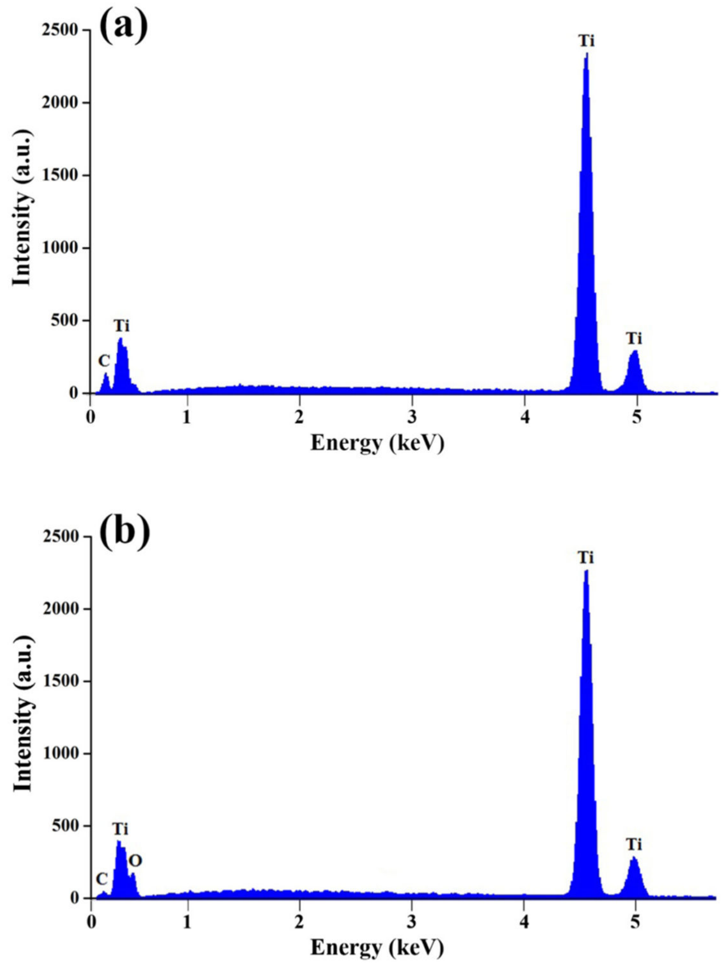

Fig. 3.
EDS spectrum of (a) untreated, (b) EPP treated for 150 s.

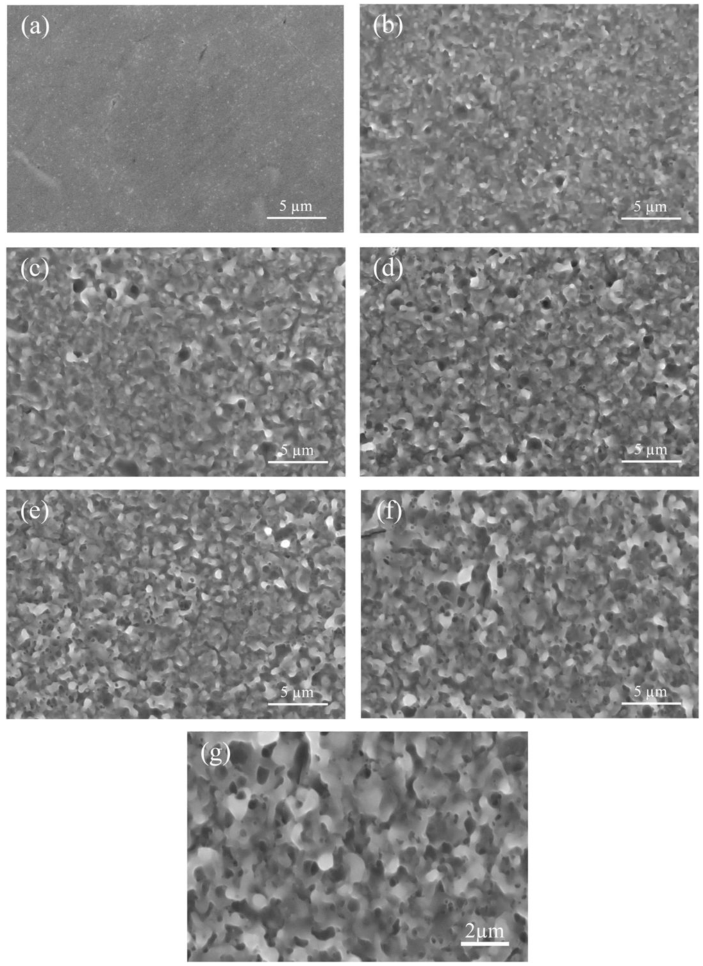

Fig. 4.

Scanning electron micrograph of EPP textured titanium (a) untreated; after processing for (b) 30 s, (c) 60 s, (d) 90 s, (e) 120 s, (f) 150 s, and (g) high magnification of (f).

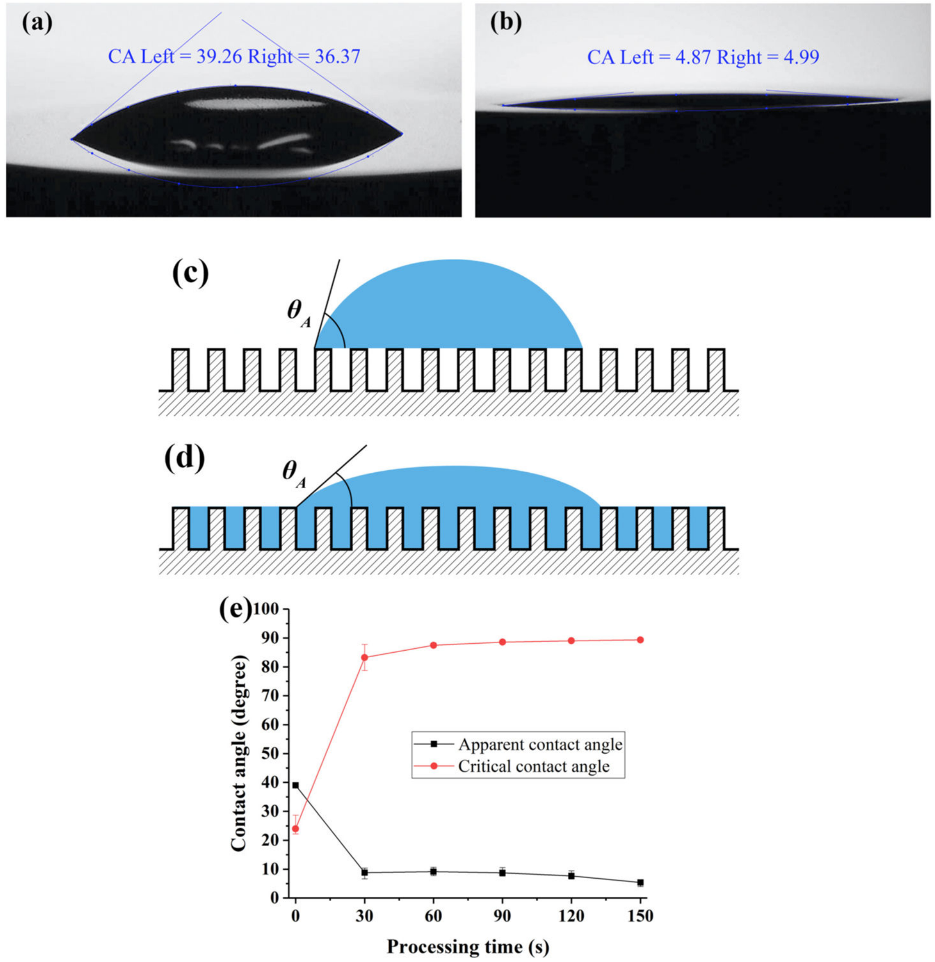

Fig. 5.

Water droplet on titanium surface (a) untreated and (b) after EPP for 150 s. Wetting of a droplet on rough surface (c) Cassie-Baxter state and (d) film state, and (e) apparent and critical contact angle as a function of EPP treatment duration.

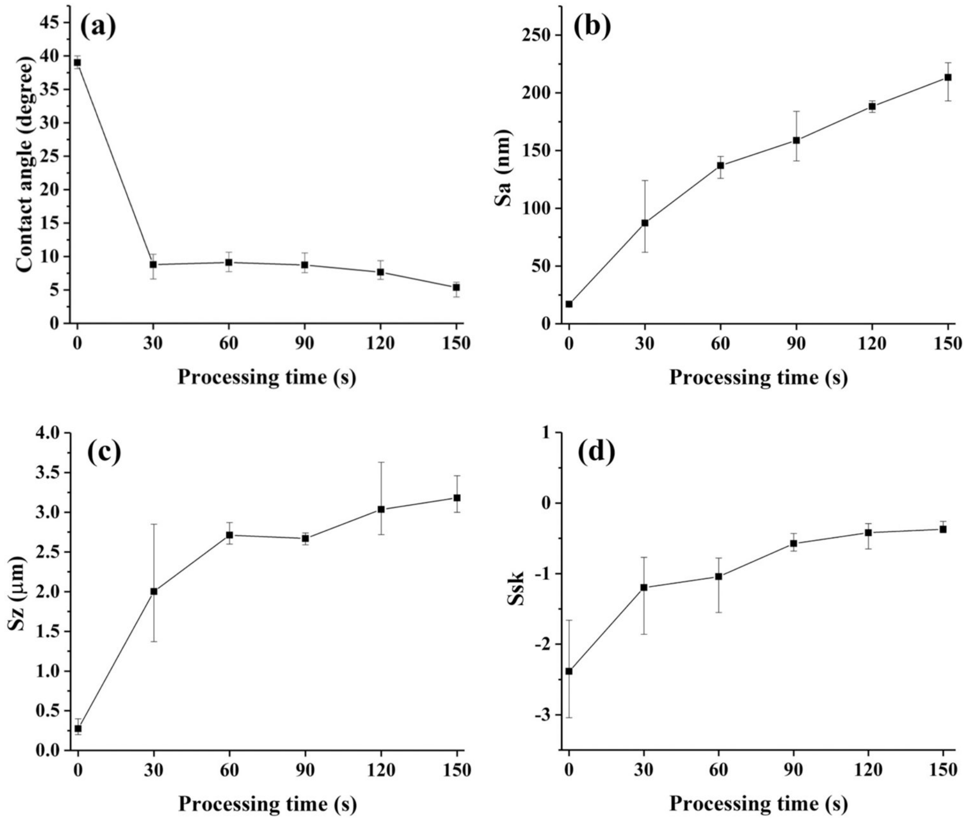

Fig. 6.

Variation of (a) apparent contact angle, (b) surface roughness (*Sa*), (c) average of maximum height from hills to valleys (*Sz*), and (d) profile symmetry about mean plane (*Ssk*) as a function of EPP processing time.

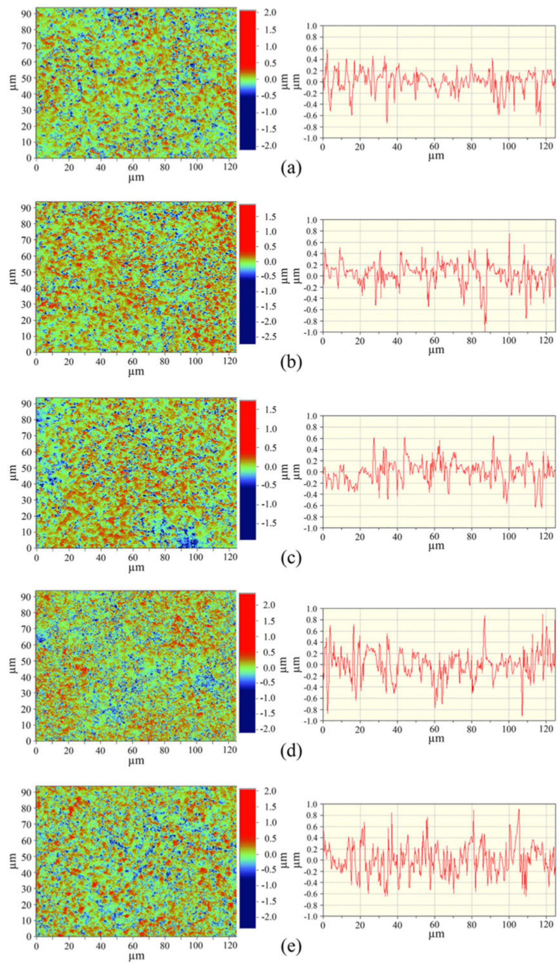

Fig. 7.

Contour spectral images (left) and 2D line scans (right) of EPP profiles after treated for (a) 30 s, (b) 60 s, (c) 90 s, (d) 120 s, and (e) 150 s.

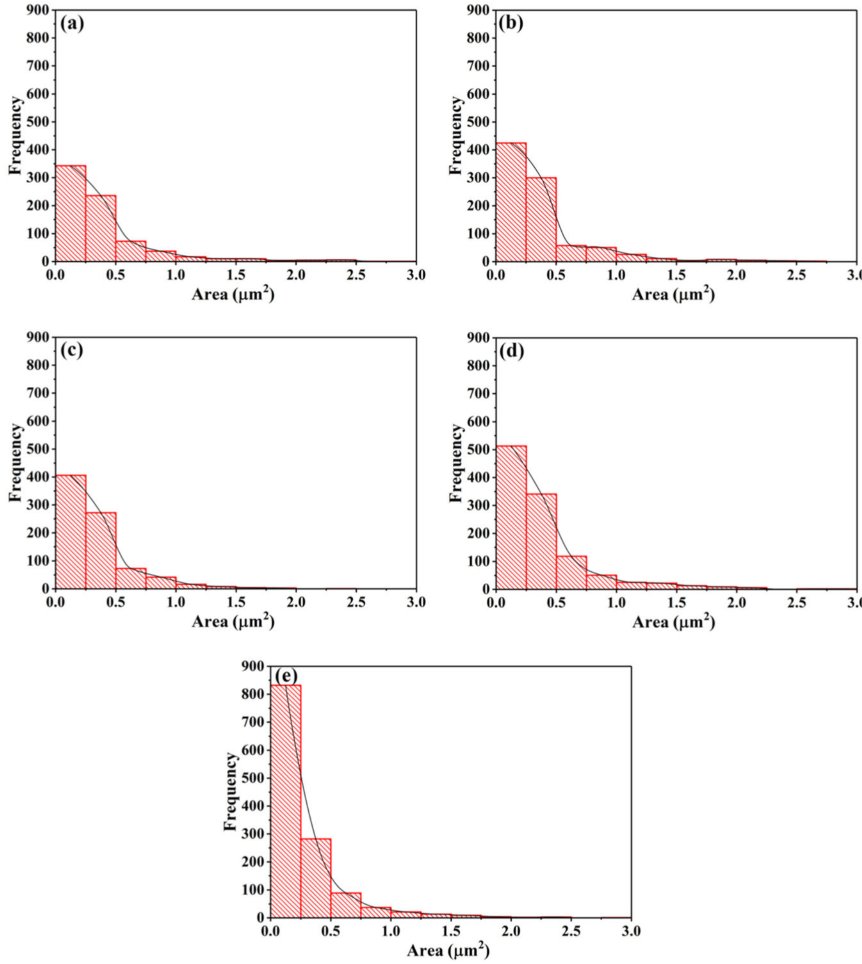

Fig. 8.

Distribution of cross-sectional area of spikes with a height of at least 0.4 μm, representing surface remaining dry for an EPP treatment of (a) 30 s, (b) 60 s, (c) 90 s, (d) 120 s and (e) 150 s.

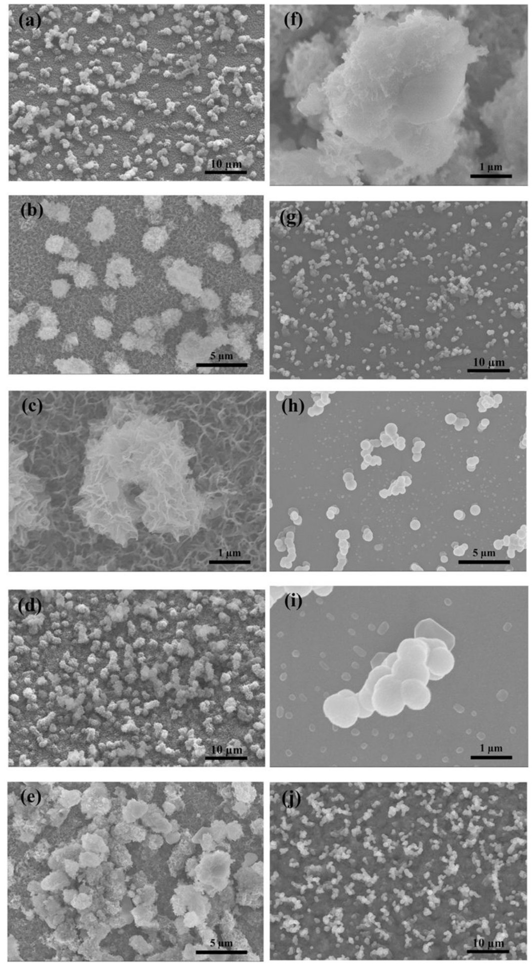
(a)
10 µm
(f)
1 µm
(b)
5 µm
(g)
10 µm
(c)
1 µm
(h)
5 µm
(d)
10 µm
(i)
1 µm
(e)
5 µm
(j)
10 µm

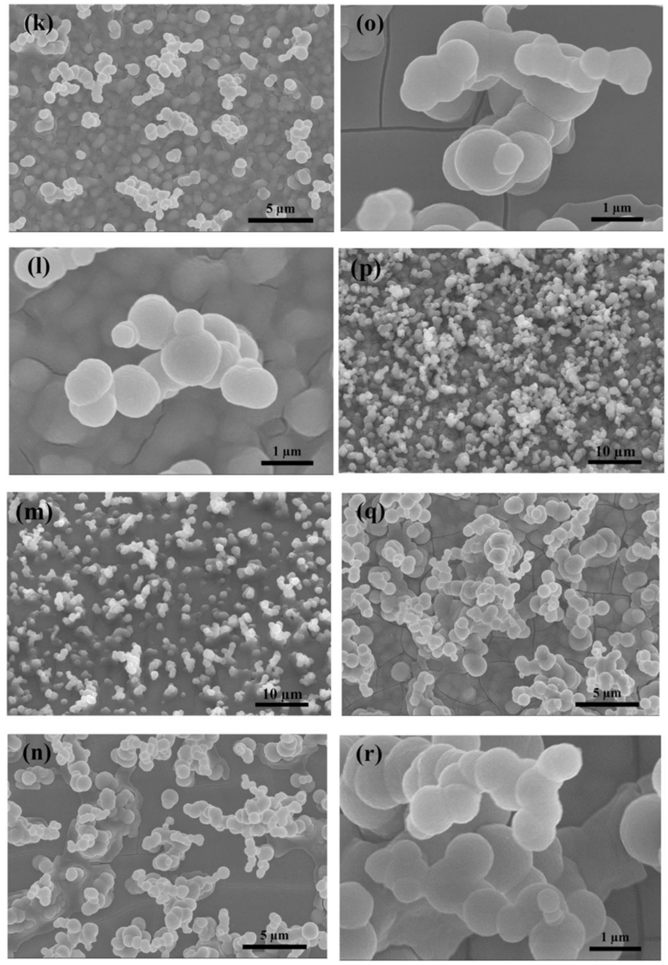

Fig. 9.

SEM images of untreated Ti after immersed in α-MEM for (a, b, c) 7 days, (g, h, i) 14 days, (m, n, o) 21 days, and EPP treated Ti 150 s after immersed in α-MEM for (d, e, f) 7 days, (j, k, l) 14 days and (p, q, r) 21 days.

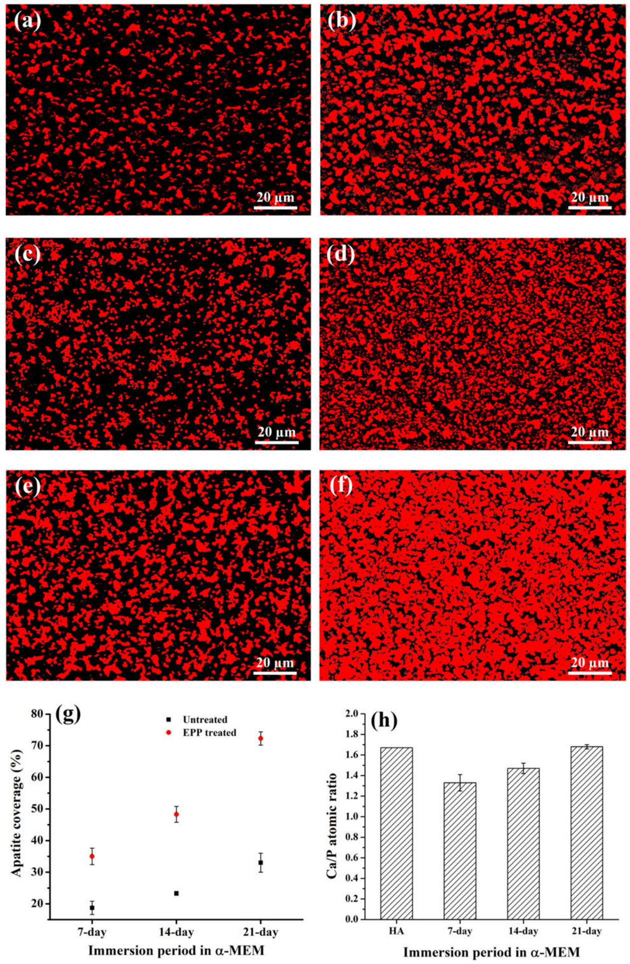

Fig. 10.

Apatite coverage on untreated Ti after immersion in α-MEM for (a) 7, (c) 14, (e) 21 days, EPP treated Ti after immersion in α-MEM for (b) 7, (d) 14, (f) 21 days, (g) percentage of apatite coverage, and (h) Ca/P atomic ratio of the stoichiometric HA and the EPP treated Ti after immersion in α-MEM.

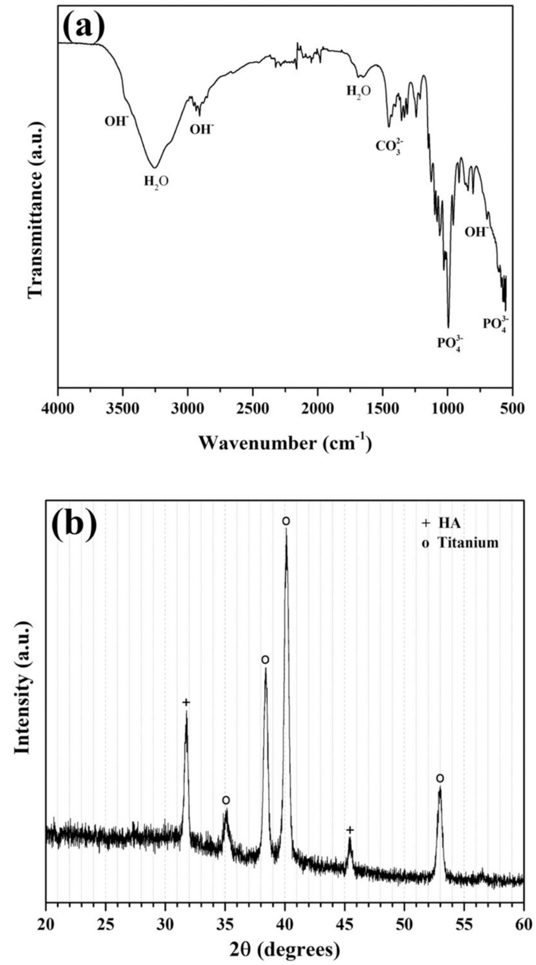

Fig. 11.
(a) FTIR spectrum and (b) XRD of EPP treated Ti for 150 s after immersion in α-MEM for 21 days.

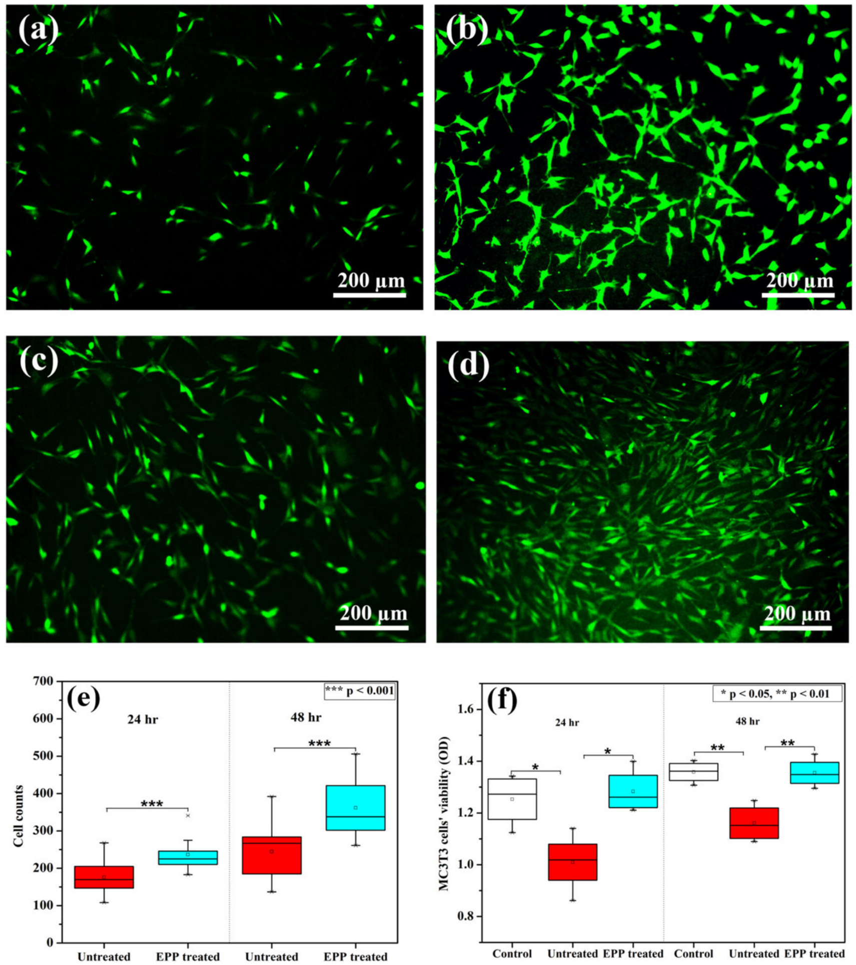

Fig. 12.

Cells attachment and viability on the Ti-surfaces, (a) and (c) show live cells on the untreated Ti surface after 24 and 48 h, respectively, (b) and (d) show live cells on the EPP treated Ti surface after 24 and 48 h, respectively. (e) and (f) present the cell counts and MTS assay results after 24 and 48 h, respectively.

Table 1

Values of the ratio of the actual surface area to the projected area (r) and fractal area of solid surface remaining dry (φ) as a function of processing time.

Parameter	Processing time (s)					
	0	**30**	**60**	**90**	**120**	**150**
r	1.10	12.40	23.20	41.20	60.40	88.60
Standard deviation	0.03	9.04	5.93	9.86	14.89	19.79
φ	0	0.031	0.036	0.041	0.042	0.046
Standard deviation	0	0.006	0.004	0.006	0.005	0.004